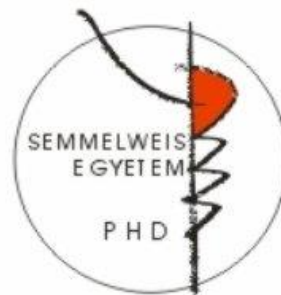


Electrophysiological analysis of the ketamine/xylazine-induced thalamocortical slow wave activity recorded in vivo in rats

Doctoral theses

Fiáth Richárd Balázs

Semmelweis University
János Szentágothai Doctoral School of Neurosciences



Supervisor: Dr. Ulbert István, DSc.

Official reviewers: Dr. Bódizs Róbert, dr. habil.
Dr. Détári László, DSc.

Chair of the Final Exam Committee: Dr. Kamondi Anita, DSc.
Members of the Final Exam Committee: Dr. Arányi Zsuzsanna, Ph.D.
Dr. Czurkó András, Ph.D.

Budapest
2016

1. INTRODUCTION

Sleep is among the most fundamental human needs. We spend almost one third of our life in this altered state of consciousness, where several physiological indicators of our body change significantly compared to the awake state. Perhaps the most striking changes take place in our brain. During sleep onset, fast brain rhythms (gamma, beta) characteristic to the awake and attentive person are gradually replaced by slower waves (alpha, theta). During the deepest stage of sleep, the majority of neurons in the brain show membrane potential oscillations with a frequency near 1 Hz; several hundred millisecond long periods with strong synaptic and spiking activity alternate with periods of near silence having similar durations.

During my doctoral work, I investigated the slow-wave activity (SWA; or also called slow oscillation) which emerges in slow-wave sleep or is induced by certain types of general anesthetics in the neocortex of rats. SWA can be recorded in vivo during natural sleep, under anesthesia and during quiet wakefulness, but can be induced in cortical and thalamocortical brain slices in vitro as well. Furthermore, it can also be detected in vivo in isolated cortical slabs of different sizes. SWA can be recorded in several brain structures, it is present virtually in every cortical region (both in glial cells and neurons), in the thalamus (almost in every thalamocortical and reticular neuron), in the hippocampus, in the basal ganglia, in the cerebellum and in the amygdala. Also, there are clusters of neurons located in several brain regions which show rhythmic activity with 1 Hz frequency in correlation with the SWA.

During SWA the membrane potential of neurons fluctuates between two states: a depolarized state (where the membrane potential is closer to the firing threshold) alternates with a hyperpolarized state (with a decreased membrane potential compared to the mean resting membrane potential and with virtually no spiking activity). The depolarized state is called up-state or active phase, while the hyperpolarized state is known as down-state or inactive phase. During up-states the local field potential (LFP) recorded with laminar multielectrodes from the neocortex of cats and rats has positive amplitude in the supragranular layers, while it is negative in deeper cortical layers. The opposite is true for down-states: close to the cortical surface we can record LFP with negative amplitudes, while in the infragranular layers down-states are positive. Up-

states may group faster oscillations like sleep spindles or gamma rhythms, while no faster oscillations can be observed during down-states.

SWA behaves like a travelling wave, slow waves may start at any point of the cortex and may propagate in any direction within this brain structure. This feature of the SWA was observed both in rats and humans. In human studies using high-density EEG it was shown, that despite the random starting position and propagation direction of slow waves, these started most frequently in frontal regions and showed an anteroposterior propagation from frontal brain regions to posterior cortical areas. Similar wave propagation patterns were observed in animal models as well.

Slow oscillation emerges spontaneously under anesthesia and in the deep stage of natural sleep, but individual cycles of the slow rhythm can be evoked with external stimulation. In previous studies it was found, that acoustic stimulation may drive the slow oscillation in thalamus, that is, acoustic stimuli delivered with a frequency similar to the peak frequency of the slow oscillation evoke up-states with high probability. As a result of the stimulation, the cycles of the SWA are phase-locked to the stimuli. SWA can be induced with transcranial magnetic stimulation and acoustic stimulation in humans, and with electric, optogenetic and somatosensory stimulation in rats. Slow waves evoked with transcranial magnetic stimulation had similar morphological features than spontaneously occurring slow waves and their propagation properties were comparable as well.

Traditionally, the slow oscillation is thought to be generated in the neocortical networks for the following reasons. First, it survives in the neocortex after thalamectomy, but cannot be recorded in the thalamus after decortication. Furthermore, the abolition of intracortical synaptic connections will result in the significant decrease of the synchronization between distant cortical areas. However, scientific evidence obtained in the recent years questioned the pure cortical origin of the SWA. Several scientific groups found that the thalamus may have a significant role in the mechanisms underlying SWA. Activity very similar to the SWA can also be recorded in thalamic brain slices, if the metabotropic receptors of thalamocortical or reticular neurons are activated. According to a recent hypothesis, three brain structures are responsible for the generation of the SWA: cortical networks, thalamocortical neurons located in thalamic nuclei and the neurons of the reticular thalamic nucleus. The cooperation of these three,

independent oscillators is necessary for the expression of the physiological slow oscillation.

Among others, SWA may have a significant role during memory consolidation and in synaptic plasticity mechanisms. Also, some sleep disorders manifest during this stage of sleep, for example sleep walking (somnambulism) or night terrors (pavor nocturnus). The SWA shows complex spatiotemporal dynamics: in the cortex it propagates horizontally between cortical areas and vertically between cortical layers, but a thalamic spreading of unit activity can also be observed. Neurons located in different cortical layers may have different roles in the genesis and shaping of the SWA, therefore laminar analysis of the neural activity during cortical slow waves may reveal novel and important mechanisms.

2. AIMS

Slow wave activity plays a significant role in several physiological functions, such as the consolidation of memory traces acquired during previous awake periods. Therefore, the understanding of mechanisms underlying SWA is an important mission of sleep research and neuroscience.

It was shown in experiments conducted recently, that the active phase of the slow oscillation starts most frequently in the infragranular layers of the rat and cat cortex. However, there is strong scientific evidence suggesting that, besides the neocortex, the thalamus also has an active role in shaping and maintaining slow waves. Latter brain structure has strong, reciprocal connections with the neocortex: thalamocortical cells make synaptic contacts mostly with neurons located in layer IV of the primary sensory cortical areas and get afferents from cortical layers V and VI. Based on these facts, we may hypothesize that, besides spontaneously occurring up-states starting in the infragranular layers, up-state related unit activity may also start in the granular layer as the result of thalamic activity.

During my doctoral studies, I examined the slow wave activity with electrophysiological methods. SWA was recorded from the somatosensory cortex of rats anesthetized with ketamine/xylazine. I investigated the participation of different cortical layers in the generation of SWA by analyzing the recorded local field potentials and unit

activity. The results obtained here were supported by thorough histological examinations.

Based on the above, we had the following aims during our experiments:

1. We determined the laminar distribution of the generators of the ketamine/xylazine-induced slow wave activity by analyzing the local field potential (LFP), local field potential gradient (GRD), current source density (CSD) and multiple-unit activity (MUA). Slow waves were recorded from the trunk and hindlimb region of the primary somatosensory cortex of rats. In order to examine whether there are duration-specific differences in the laminar distribution of the generators, up-states were divided into three distinct groups based on their duration.
2. In the same cortical regions, we examined the laminar distribution of up-states evoked with mechanical somatosensory stimulation. CSD and MUA traces were used for the analysis and the results were compared with the results obtained with the analysis of spontaneously occurring up-states.
3. Based on the MUA, we examined in which cortical layers spontaneously occurring and evoked up-states started most frequently.

3. MATERIALS AND METHODS

3.1 Animal surgery and anesthesia

Twenty Wistar rats (average: 308±88 g, range: 180-460 g, gender balanced) were used for the acute experiments. All experiments were performed according to the EC Council Directive of November 24, 1986 (86/89/EEC) and all procedures were reviewed and approved by the local ethical committee and the Hungarian Central Agricultural Office (license number: 22.1/4228/003/2009). Animals were anesthetized with a mixture of ketamine and xylazine administered intraperitoneally at 2 ml/kg body weight injection volume. Supplementary intramuscular ketamine/xylazine injections

were given to maintain the depth of anesthesia during the recording sessions. After preparing the craniotomy, the recording probe attached to a manual microdrive was moved to the target location (trunk (S1Tr) or hindlimb (S1HL) region of the primary somatosensory cortex) and inserted slowly to a depth of approximately 3 mm below the dura mater with guidance of a surgical microscope.

3.2 Multielectrodes and electrophysiological recordings

The electrode used to record brain electrical activity had a 7 mm long silicon-based shaft, with an 80x280 μm thickness, and had 24 square-shaped (30x30 μm) platinum contact sites with 100 μm intercontact distances. The first contact was located 660 μm away from the tip of the probe. Two stainless steel needles inserted into the left and right side neck muscles of the animal served as reference and ground electrodes. The brain signals were amplified and filtered (gain: 1000, band-pass: 0.1-7000 Hz) by a custom-made headstage and amplifier, and were digitized with 20 kHz/channel sampling rate, on 24 channels at 16-bit precision. The recordings were carried out with custom-written LabVIEW software and stored on the hard drive of a PC for offline analysis. 15-minute-long data segments were recorded and a recording session lasted about 3-5 hours. In several experiments, the recording was followed by administering a small positive current (1.5 μA) for 1-2 minutes through three or four recording sites with well-defined distances from each other to form electric lesions and to accurately determine the relationship between recording sites and cortical laminae. We did not record the signals coming from the most dorsal contact site, the recording channel corresponding to this contact site (24th channel) was reserved for the registration of the trigger signal containing the delivery time of the somatosensory stimuli. We also examined whether the type, material or geometry of the recording probe has an influence on the recorded data or the results. To assess this issue, we performed several experiments using two types of linear multielectrodes which had different parameters than the silicon-based recording probe (stainless steel multielectrode: n = 5 experiments; SU-8 polymer-based multielectrode: n = 4 experiments).

3.3 Somatosensory stimulation

A custom-made mechanical stimulator, based on a stepper motor, was used to stimulate the skin on the trunk or on the hindlimb of the animal. The parameters of the stimulation were controlled externally through a custom-made LabVIEW software.

Duration of the pulses was either 50 or 100 ms, which represents the period of time during which the stick reaches the skin of the animal, touches it and returns to the starting position. The stimulation frequency was set to 1.5 Hz, based on the average peak frequency of ketamine/xylazine-induced SWA measured in our previous experiments. In one experiment, the interstimulus intervals were selected randomly from the 0.5-0.7 s range (corresponding to the 1.43-2 Hz frequency range). The moving end of the stimulator was placed 5 mm far from the skin of the rat for tapping stimulation. Angular velocities corresponding to the stimulus durations were 400°/s and 200°/s, respectively. Stimulus delivery times were obtained from the trigger channel which recorded the stimulation pulses.

3.4 Histology

After the recording session the multielectrode was withdrawn and the animal was deeply anesthetized and perfused through the heart first with physiological saline (100 ml) followed by 4% paraformaldehyde in 0.1 M phosphate buffer (pH=7.4, 300 ml). The brain was removed and post-fixed overnight at 4 °C. The fixed brain was sectioned using a vibratome (Leica VT1200) into 60 µm thick coronal sections. Following washing in 0.1 M phosphate buffer, sections were mounted from gelatin, air dried, processed for cresyl violet (Nissl) staining, dehydrated in xylene and coverslipped with DePex. The sections were photographed under an Axioplan 2 microscope equipped with a DP70 digital camera to examine the track of the silicon probe, to verify the recording position and to determine the boundaries between cortical layers. In case of several experiments the probes were dipped in red-fluorescent dye (DiI) to accurately determine the position of the tip of the probe in the brain tissue.

3.5 Data analysis

Detection of cortical up- and down-state onsets. The algorithm used to detect state onsets was the following: we separated the MUA signal from the wideband data by filtering (band-pass filter, 500-5000 Hz, zero-phase shift, 24 dB/octave, rectification). Signals were downsampled from 20 kHz to 2 kHz for faster processing. The envelope of the downsampled MUA was extracted with an additional low-pass filter (zero-phase shift, 30 Hz, 24 dB/octave). After the filtering step, the values on the 23 channels were summed resulting in one trace representing the instantaneous intensity of summated population activity (SPA) in the examined cortical area. The amplitude histogram of the

SPA showed a clear bimodal distribution. The threshold value to determine the up- and down-state onsets was calculated, as follows. The time points corresponding to the LFP peak of 50 randomly selected down-states (lack of MUA) longer than 100 ms were marked manually on the SPA trace and the average (AVG) and standard deviation (SD) of the selected values were calculated. The threshold level was set to $AVG + (3 * SD)$. With lower threshold levels the algorithm may detect spurious up-state onsets within down-states, while higher threshold values can cause an inaccurate detection of state onsets. Based on empirical observations, the minimum duration of an up-state was set to 50 ms in the state detection algorithm, while the duration of a down-state was chosen to be minimum 100 ms. The onset of an up (down)-state was defined as the time point at which the value of the SPA trace exceeded (fell below) the calculated threshold level. This time point had to be preceded by an opposite state with a length equal to or longer than the defined minimal state length.

Estimation of the LFP gradient and the CSD. The LFP was obtained from the wideband data by filtering (band-pass filter, 0.3-500 Hz, zero-phase shift, 24 dB/octave). The GRD, which is the first spatial derivative of the LFP, was estimated by the voltage difference between consecutive recording sites. CSD analysis reveals synaptic/transmembrane generators of the LFP in laminated neural structures and is calculated as the negative second spatial derivative of the LFP. The following three-point formula was used for the approximation of the CSD:

$$CSD_j = -(u_{j-1} - 2u_j + u_{j+1})/rh^2,$$

where u_j is the LFP in μV at a given recording site j , r is the resistivity of the tissue in $\Omega \cdot cm$, and h is the distance between recording sites (100 μm in our case). We assumed homogeneous tissue resistivity and both r and h were substituted by the dimensionless number 1 in the calculations. High spatial frequency noise and boundary effects were reduced by Hamming-window smoothing and interpolation. Both signal types were expressed in microvolts.

Detection of up-state onsets in different layers. We aimed to locate the neocortical layer where cell firing starts during up-states. To achieve this, we detected up-state onsets on every channel separately, except those with low MUA levels. Channels showing low firing activity were located in layers I, II and the bottom part of layer VI. These channels were disregarded from this analysis to avoid inaccurate results.

Individual threshold levels were calculated for every channel, which were the sum of the average of down-state amplitudes on the actual channel (AVG_j , where j is the channel number and $j = 1, \dots, 23$) and a constant value (C) obtained empirically. $AVG_j + C$ resulted in similar threshold levels between the channels. The channel showing the largest fluctuations in the MUA level between up- and down-states (usually a channel located in cortical layer V with strong unit activity) was chosen as the reference channel. The time point corresponding to every up-state onset detected on the reference channel was then compared to the up-state onsets detected on the other investigated channels in a 300 ms time window and the channel with the earliest up-state onset was selected. Channels were then assigned to the appropriate cortical layers and the probability of up-state initiation indexed by MUA was calculated in each layer.

Time-frequency analysis. The relative spectrograms were computed with wavelet analysis from LFP epochs cut from the continuous traces. Epochs were ten second long, with the state onset located in the middle. We selected the baseline as the first 500-ms-long interval of the ten-second-long epochs. On the spectrogram only a 1300-ms-long section of the full epoch is shown, which consists of a 500-ms-long interval before the state onset and 800-ms-long interval after the state onset.

Analysis of up-states evoked with somatosensory stimulation. In this study, we used mechanical somatosensory stimulation to evoke up-states in the somatosensory cortex of anesthetized rats. To obtain stimulus-evoked up-states from the recordings, first we detected the state onsets with our detection algorithm. We constructed peristimulus time histograms (PSTHs) using the delivery time of stimuli and the onset of detected up-states. The PSTHs showed us the quantity of evoked up-states and their latency compared to the start of the stimulus. We separated stimulus-evoked up-states from spontaneous ones as follows. Evoked up-states should have started in the interval of 10-60 ms after the onset time of the stimulus (stimulus delivered during the down-state) and had a minimum duration of 50 ms (the minimum duration of up-states set in our state detection algorithm). The 10-60 ms interval was selected empirically, after inspecting peristimulus time histograms showing the relation of the delivered stimulus and up-state onsets. All remaining up-states were considered spontaneously occurring up-states. After grouping, evoked up-states and spontaneous up-states were analyzed

separately. Finally, CSD and MUA depth profiles of evoked up-states and spontaneously occurring up-states were constructed and compared.

4. RESULTS

4.1 Distribution of the phase durations of spontaneously occurring ketamine/xylazine-induced slow wave activity recorded in the rat somatosensory cortex

Based on our data, up-states had an average duration of 292.77 ± 111.73 ms (range: 50-894 ms), while down-states were on average 305.29 ± 94.17 ms long (range: 100-819 ms). The average duration of a complete slow-wave cycle was 601.73 ± 162.15 ms (range: 151-1473 ms). Based on their duration, detected up-states were separated into three groups and analyzed independently: brief (50-200 ms), average duration (200-400 ms) and long (> 400 ms) up-states. Besides these groups, we also analyzed down-states with a duration between 200 and 400 ms.

Most of the detected up-states ($n = 35520/56263$, 61.8%) had an average duration, 20.4% ($n = 11629$) were brief up-states, and the remaining 17.8% ($n = 9114$) belonged to the group of long up-states. After artifact rejection and data cleansing (only up-states preceded and followed by down-states with a minimum length of 200 ms were further analyzed to avoid sections of the recordings containing faster oscillatory activity) the number of up-states described above decreased by an amount of about 30% (average duration up-states: $n=24513$, 66.6%; brief up-states: $n=5434$, 14.8%; long up-states: $n=6858$, 18.6%). We did not find significant differences between the results obtained from the trunk and hindlimb region, therefore we merged all data.

4.2 The thickness of layers in the investigated somatosensory cortical areas

Because we determined the relationship between the recording sites and the cortical layers mainly based on postmortem histology, it is necessary to estimate the change of the tissue size of coronal brain sections related to histological procedures. To obtain the degree of tissue shrinkage or expansion in our case, we measured the change of the tissue size in the coronal plane along the mediolateral (x) and the dorsoventral (y)

axes. To calculate the change in the x-axis, at the end of the experiment the retracted recording probe was reinserted laterally or medially into the brain tissue to well-defined distances, parallel to the first insertion track. Afterwards, the distance between the two penetrations was measured on the Nissl-stained sections at two different positions which were separated at least 500 μm apart from each other. The two distance values were averaged and compared with the known shift value. The size change in the y-axis was obtained by first measuring the spatial interval between the centers of adjacent electrical lesions visible on the Nissl-stained sections. The measured distance was then compared with the actual distance between those contact sites which were selected to induce these lesions.

Our thorough anatomical analysis revealed that the brain tissue showed a swelling of ~2 to 3% following histological procedures, both along the dorsoventral ($2.42\pm 5.3\%$) and the mediolateral ($2.76\pm 4.68\%$) axis. This would not substantially affect the results of our laminar analysis, and therefore, we did not apply any correction factor.

The six layers of the cortex were identified in Nissl-stained cortical sections. In the somatosensory cortex, layer I was a bright and cell-sparse area below the meninges and was approximately 150 μm thick (trunk region of the primary somatosensory cortex (S1Tr): $137\pm 23\ \mu\text{m}$; hindlimb region of the primary somatosensory cortex (S1HL): $160\pm 23\ \mu\text{m}$). This was followed by the thin, cell-dense layer II (S1Tr: $88\pm 20\ \mu\text{m}$; S1HL: $95\pm 16\ \mu\text{m}$). Layer III had an average thickness of around 400 μm (S1Tr: $375\pm 56\ \mu\text{m}$; S1HL: $401\pm 59\ \mu\text{m}$). This layer contains mainly pyramidal cells and is usually merged together with layer II due to the lack of a clearly visible border between them. The thalamorecipient layer IV comprising a high number of spiny stellate cells, was an about 150 μm thick, darker band located below layer III (S1Tr: $146\pm 29\ \mu\text{m}$; S1HL: $143\pm 18\ \mu\text{m}$). This was followed by layer V containing the cell bodies of the largest pyramidal cells in the rat somatosensory cortex. Layer V can be divided into two sublayers, the thinner and cell-sparsier layer V/A (S1Tr: $142\pm 36\ \mu\text{m}$; S1HL: $153\pm 24\ \mu\text{m}$) containing predominantly slender-tufted pyramidal cells and the approximately 300 μm thick, cell-dense layer V/B (S1Tr: $300\pm 59\ \mu\text{m}$; S1HL: $347\pm 64\ \mu\text{m}$), mostly with a mixture of slender and thick-tufted pyramidal cells. Lastly, layer VI, found most ventrally and directly above the white matter, was the thickest of all the layers, with an average thickness of more than half a millimeter (S1Tr: $589\pm 91\ \mu\text{m}$; S1HL: 669 ± 136

μm). We found a significant difference between the thickness of the two investigated areas, the S1Tr ($1777\pm 160\ \mu\text{m}$) and the S1HL ($1969\pm 161\ \mu\text{m}$, $p=0.0009$), which was caused predominantly by the thickness difference of layer V/B ($300\ \mu\text{m}$ vs. $347\ \mu\text{m}$, respectively, $p=0.0243$) and layer VI ($589\ \mu\text{m}$ vs $669\ \mu\text{m}$, respectively, $p=0.036$) between the two regions.

4.3 Spectral properties of the ketamine/xylazine-induced spontaneous slow wave activity

The frequency of SWA under ketamine/xylazine anesthesia is somewhat higher compared to slow waves observed during natural slow-wave sleep and is usually more regular and rhythmic. We measured an average peak frequency of $1.5\pm 0.26\ \text{Hz}$ (range: $1.098\text{-}1.952\ \text{Hz}$) during our experiments. This result was comparable to peak frequencies of the ketamine/xylazine-induced SWA found in rats by other groups. The laminar FFT power spectrum profile in the frequency range of the SWA ($0.6\text{-}4\ \text{Hz}$) was calculated from the LFP and from the GRD. The profile was constructed by the spatial interpolation of the FFT power spectrum between cortical channels in the $0.6\text{-}4\ \text{Hz}$ frequency band (cubic spline interpolation). The power of slow wave activity in the LFP was the strongest in layer I, IV and V, while it was lower in layer III and layer VI. The GRD power spectrum had two peaks, dominating in layer III and layer VI. This indicates that the LFP amplitude change between adjacent sites is maximal in these layers.

4.4 Correlation and coherence of the slow wave activity between layers of the somatosensory cortex

To examine the laminar distribution of the ketamine/xylazine-induced slow waves in more detail we calculated the pairwise linear correlation and coherence between each LFP channel and also between each GRD trace. The coherence was computed in the $0.6\text{-}3\ \text{Hz}$ band. The depth distribution profile of the pairwise coherence and correlation of the LFP showed high values between adjacent channels. Analyzing the depth profile of the pairwise coherence and correlation of the GRD channels demonstrated that there is a strong coupling within supragranular (I-III), granular (IV)

and infragranular (V-VI) layers, but a considerable coherence was also confirmed between layer VI and layers II-III. The weakest values were found between layer V and the supragranular layers.

4.5 Laminar depth profiles of spontaneously occurring up-states with average duration recorded in the somatosensory cortex

After the detection of up-state onsets, 1300-ms-long epochs were cut from the continuous signals, with a 500-ms-long section before the up-state onset and an 800-ms-long section after the onset. Up-state onset locked averages were calculated from the LFP, GRD, CSD and the MUA traces and channels were assigned to the appropriate cortical layer. Color maps were constructed from the average traces using spatial interpolation between neighboring channels. Activity in the somatosensory cortex during up-states was frequently modulated by thalamocortical sleep spindles (10-16 Hz). Spindle cycles consisted of short (~40ms), alternating phases of stronger and weaker MUA. Average duration up-states contained three or four of these spindle cycles, but usually these were not visible on the averages, since they were not time locked to the up-state onsets.

Normalized grand averages were calculated from all experiments at two relevant phases of the up-states. The initial period of the up-state (termed as “up-state initiation”, representing a 25-ms-long time interval starting 25 ms after the up-state onset) was chosen because of the strongest currents and strongest MUA observed during this time interval. The other phase of the up-state, termed as “up-state peak”, representing a 50-ms-long time interval starting 125 ms after the up-state onset, and corresponding to the positive LFP peak recorded in layer I during up-states was also investigated. The samples comprising the examined phases were averaged together within every channel. Next, the obtained values were averaged between the channels corresponding to the same cortical layer. Finally, these values were normalized and averaged between experiments. In case of the MUA, the background noise was calculated on every channel before normalization by averaging the MUA at the LFP peak of 50 randomly selected down-states (no unit activity). These noise values were then subtracted from the obtained MUA values.

A negative potential deflection was apparent in the depth profile of the LFP during the start of the up-state with an amplitude peak in layer IV and a polarity change in layer VI. After approximately 50 ms, the field potential inverted into positive polarity in the superficial layers and remained positive until the subsequent down-state. The positive-negative polarity shift at the peak of the up-state was located at the top of layer III, close to the border of layer II and III. Below the supragranular layers the LFP amplitudes of up-states were negative. Analyzing the GRD revealed a positive deflection with a layer II peak shortly after the up-state onset which turned negative below the supragranular layers. The negative amplitude GRD had the strongest value in layer V. This deep negativity changed into positivity at the peak of the up-state in layer IV and in layer V/A as well, remaining negative only in layers V/B and VI. The depth profile of the CSD indicated a broad and strong current sink (inward current) during the beginning of up-states, principally in layer III and IV, invading also the upper segment of layer V. We found that this presumably active sink was surrounded by two current sources (outward current), one stronger on the cortical surface (layer I) and another weaker with a shorter duration in layer VI. This latter source vanished at the peak of the up-state, while the upper, layer I source persisted through the whole up-state. The strength of the sink decreased with the progression of the up-state and it shifted to deeper cortical layers. The MUA depth profile of up-state onset locked averages showed that the strongest MUA was formed in layer V/B and the amplitude of the activity decreased both in the ventral and dorsal directions as a function of distance. In layer I and II we found only barely measurable MUA. At the beginning of the up-state, the MUA was approximately 30% stronger in every layer compared to the activity measured at the peak of the up-state. Both the depth profiles of the CSD and the MUA suggest that neuronal activity was the strongest during the first 50 ms of the up-state which corresponds to the first spindle cycle. After the first 50 ms, the synaptic and spiking activity decreased with the progression of the up-state.

When we determined up-state onsets for every channel separately, we found that MUA started in layer V during the majority of up-states, in most cases. The initiation of up-states was associated with a weak current sink located in layer V accompanied with early MUA in the same layer on the up-state onset locked averages. Average spectrograms constructed from up-state onset locked epochs and computed in each layer

showed a strong power increase in the 0.6-100 Hz frequency range during up-states, while a decrease in spectral activity could be observed during down-states, in agreement with previous data.

4.6 Laminar depth profiles of brief and long up-states recorded in the somatosensory cortex

We found only minor quantitative differences between depth profiles of spontaneously occurring brief, long and average duration up-states. The laminar distribution of MUA and CSD depth profiles of brief and long up-states were very similar to depth maps of 200-400 ms long up-states, both during the onset and at the peak of up-states. During the up-state onset a source-sink-source configuration was visible on the up-state-locked averaged depth profiles of both brief and long active phases. However, the source located in deep cortical layers during brief up-states appeared with a smaller intensity on the depth profile compared to the deep source during longer up-states. Similar to what we have observed during the up-states with average duration, brief and long up-states started most frequently with a sink located in layer V, and unit activity was also initiated in this particular layer with the activity propagating to supragranular and deeper layers.

4.7 Laminar analysis of spontaneously occurring down-states

Compared to the results obtained with the analysis of up-states, the major difference between the laminar analysis of spontaneously occurring down-states was in the unit activity. In agreement with scientific data of other groups, no unit activity could be detected during down-states in none of the cortical layers, neither at the down-state onset, nor at the peak of the inactive phases. Based on the down-state onset-locked, averaged CSD depth profile, the first current source appeared in layers III-IV, which was shortly followed by a current sink located ventrally. A couple of milliseconds later the source-sink pair was supplemented by another current sink, which was located at the surface of the cortex. This sink persisted until the end of the down-state. The deep cortical current sink disappeared after the first 100 ms and the current source found in the granular layer shifted to deeper layers.

4.8 Laminar analysis of up-states evoked with somatosensory stimulation

In a subset of experiments rhythmic mechanical somatosensory stimulation was applied on the skin of the trunk or the hindlimb of the animal either with stimulation frequency similar to the peak frequency of the ketamine/xylazine-induced SWA (1.5 Hz) or with an interstimulus interval selected randomly from the 0.5-0.7 s range. Short sensory stimuli can evoke or terminate up-states depending on the instantaneous phase of the actual state. Our stimulation protocol could reliably evoke up-states. Stimulation of the receptive field of the investigated area resulted in evoked up-state ratios of 20-30% of all detected up-states and occasionally the stimulation entrained the SWA for several seconds.

Evoked up-states were extracted from the data and their up-state onset locked CSD and MUA depth profiles were constructed. All the other up-states detected in recordings containing somatosensory stimulation were considered spontaneous up-states. Up-state onset locked CSD and MUA depth profiles of these spontaneously occurring up-states were calculated as well and compared with the depth profiles of evoked up-states. Normalized grand averages of evoked and spontaneous up-states were calculated during the up-state initiation phase (5-30 ms) and at the peak of up-states (125-175 ms). We found that during the up-state initiation phase the recorded MUA during evoked up-states was significantly stronger in all layers compared to the unit-activity during spontaneous up-states. Significant differences in the CSD were also found in layers I, III and V, mainly related to stronger currents during the evoked up-states. This phenomenon is presumably caused by the synchronous activation of neuronal populations responsible for the generation of the transient evoked response to somatosensory stimulation. These differences in the synaptic and spiking activity vanished after the first 50 ms of up-states and the calculated CSD and MUA values of the two types of up-states became similar at the peak phase of the up-state. Another remarkable difference between the spontaneous and evoked up-states was that while in the former case a source-sink-source configuration characterized the initiation of up-states in the laminar profile of the CSD, in the latter case a new current source appeared in layer V. This current source may represent the passive recurrent flow related to the strong synaptic activity in layer IV and layer III induced by sensory stimulation. The

earliest MUA onset was found in layer IV and the earliest sink was located in layer III and IV during stimulus evoked up-states, suggesting a strong thalamic contribution to these events through the thalamorecipient layer IV.

4.9 Laminar distribution of the multiple-unit activity onset during up-states

Our state detection method demonstrated that MUA during spontaneous up-states may start in any of the cortical layers (III-VI). However, two cortical layers showed higher probability of up-state related firing onset than others (layer V/B and IV). In the majority of animals, MUA started with the highest probability (> 50% of all detected up-states) in layer V/B during spontaneous activity. However, spontaneous up-states with layer IV MUA onset were found in high numbers in several experiments, exceeding the number of layer V up-states.

Furthermore, we examined the change in the laminar distribution of up-state onsets indexed by MUA in response to somatosensory stimulation. Compared to the results obtained during spontaneous activity, where mainly up-states with layer V onset dominated, the stimulation resulted in the increase of up-states starting in layer IV. This increase was accompanied by the simultaneous decrease of up-states with a MUA onset in layer V. The majority of the detected up-states with a layer IV onset came shortly after a stimulus, indicating that they may belong to the group of evoked up-states.

5. CONCLUSIONS

One of the aims of this study was to compare the results obtained in rats to the results of a human study performed earlier by our group. During up-states, a strong positivity can be observed in the depth profile of the LFP gradient located in the supragranular layers, both in rats and in drug-resistant patients with focal epilepsy. In both cases, the peak of this positivity was located in cortical layer II. However, while the LFP gradient during the up-state onset was dominated by negative amplitudes in the infragranular layers of rat cortex, in humans there was no significant activity in deep cortical layers. The supragranular section of the CSD depth profile showed similar patterns in both species, a strong source-sink pair was found in the upper layers. The

current source was located in layer I both in rats and humans, but the spatial distribution of the current sink was broader in rats, it could be detected in the upper segment of layer V. In humans, the outspread of the sink did not reach the bottom of layer IV. Significant differences were found in the activity of the infragranular layers, while in humans there was only weak flow of currents in layers IV-VI, another strong current source was found in layer VI of the rat cortex during the up-state onset. However, at the peak of the up-state this deep current source was exchanged by a weak sink, and the main sink shifted from the granular layer to the bottom of layer V. In humans, significant unit activity could be detected on the MUA depth profile in each layer, except layer I. MUA was the strongest in the middle layers of the cortex, with two peaks, one located in layer III and the other in layer V. The situation was different in rats, the strongest unit activity could be detected in layer V, while the activity in other layers (with the exception of layer IV) was sparse. The observed differences may be the combined result of multiple factors. Such influencing factors may be for example the different cytoarchitectonics of the investigated cortical areas (primary somatosensory cortex in rats vs. frontal and parietal cortical regions in humans), differences between natural sleep and anesthesia or phylogenetic differences (more developed supragranular layers in humans). Of course, we cannot exclude the possibility, that some of the differences observed in the human depth profiles are of pathological origin.

The results observed in our study were in many ways similar to results obtained by other research groups in different animal models (cat, rat, mouse). The acquired depth profiles were highly similar between different cortical areas (auditory cortex, somatosensory cortex) and under different conditions (natural sleep, ketamine/xylazine or urethane anesthesia). Dominant unit activity in layer V, current sink located in middle cortical layers and a current source next to the brain surface and deep layers of the cortex were characteristic to the depth profiles. However, there were also some differences which may be statistically significant.

Analyzing the population activity, we found during our experiments that the MUA of spontaneously occurring active phases of the slow oscillation could start in virtually any of the cortical layers (III-IV), but they were most frequently initiated in layer V. However, in a subset of experiments, layer IV was considerably active in initiating up-state related MUA even in the absence of somatosensory stimulation. Somatosensory

stimulation further strengthened up-state initiation in layer IV. Because layer IV is the main thalamorecipient layer in the somatosensory cortex, we may rightly assume, that the early MUA detected in layer IV during up-states is the effect of the activity of thalamocortical neurons, that is, these layer IV up-states could be initiated by the thalamus. These findings support the important role of the thalamus in the generation of the SWA.

The high number of up-states which started in layer IV were observed in the minority of experiments (in one fifth of the cases), in other cases up-states showed a frequent initiation in layer V. One of the explanation for our results may be that during breathing, the area of skin on the abdomen of the animal is stimulated rhythmically and continuously (the skin touching the heating pad), which in turn activates layer IV neurons in the investigated part of the somatosensory cortex through the thalamus. That is, these spontaneously occurring up-states with layer IV initiation may be in fact active states evoked with somatosensory stimulation.

Our results confirm that cortical layer V firing may have a major contribution to the up-state generation of ketamine/xylazine-induced SWA, however, thalamic influence through the thalamorecipient layer IV can also play an initiating role, even in the absence of sensory stimulation.

6. LIST OF PUBLICATIONS

6.1 *The author's publications related to the dissertation*

Márton G, Orbán G, Kiss M, Fiáth R, Pongrácz A, Ulbert I. (2015) A multimodal SU-8 platinum – polyimide microelectrode array for chronic in vivo neurophysiology. PLoS One, 10: e0145307

Fiáth R, Kerekes BP, Wittner L, Tóth K, Beregszászi P, Horváth D, Ulbert I. (2016) Laminar analysis of the slow wave activity in the somatosensory cortex of anesthetized rats. Eur J Neurosci, 44: 1935-1951.

6.2 *Other publications*

Grand L, Pongrácz A, Vázsonyi E, Márton G, Gubán D, Fiáth R, Kerekes BP, Karmos G, Ulbert I, Battistig G. (2011) A novel multisite silicon probe for high quality laminar neural recordings. Sensors Actuat A-Phys, 166: 14-21.

Torfs T, Aarts AAA, Erismis MA, Aslam J, Yazicioglu RF, Seidl K, Herwik S, Ulbert I, Dombóvári B, Fiáth R, Kerekes BP, Puers R, Paul O, Ruther P, Van Hoof C, Neves HP. (2011) Two-dimensional multi-channel neural probes with electronic depth control. IEEE Trans Biomed Circuits Syst, 5: 403-412.

Héja L, Nyitrai G, Kékesi O, Dobolyi Á, Szabó P, Fiáth R, Ulbert I, Pál-Szente B, Palkovits M, Kardos J. (2012) Astrocytes convert network excitation to tonic inhibition of neurons. BMC Biol, 10: 26.

Márton G, Fekete Z, Fiáth R, Baracskaý P, Ulbert I, Juhász G, Battistig G, Pongrácz A. (2013) In vivo measurements with robust silicon-based multielectrode arrays with extreme shaft lengths. IEEE Sensors J, 13: 3263-3269.

Dombóvári B, Fiáth R, Kerekes BP, Tóth E, Wittner L, Horváth D, Seidl K, Herwik S, Torfs T, Paul O, Ruther P, Neves HP, Ulbert I. (2014) In vivo validation of the electronic depth control probes. Biomed Tech (Berlin), 59: 283-289.

Kárász Z, Fiáth R, Földesy P, Vazquez A. (2014) Tunable low noise amplifier implementation with low distortion pseudo-resistance for in vivo brain activity measurement. IEEE Sensors J, 14: 1357-1363.